Cluster-Assembled Nanocomposites: Functional Properties by Design

Cahit Benel,* Thomas Reisinger,* Robert Kruk,* and Horst Hahn*

The unique functional properties of nanocomposites meet many of the material requirements sought after in numerous applications of today's high-tech industry. This, in turn, inspires material scientists to devise new methods that can further expand the palette of available nanocomposites. Precise control over the chemistry, morphology, and microstructure of nanocomposites' constituents promises the eventual ability to design any composite material for any specific requirement. However, today's synthesis methods still lack the ability to simultaneously control all chemical, morphological, and microstructural features of nanocomposites in a one-step process. Here, an alternative approach to fabricate fully tailorable nanocomposites under well-defined conditions is described. In particular, this progress report focuses on the combination of cluster ion beam and thin-film deposition technologies to fabricate cluster-assembled nanocomposites via codeposition of cluster ions and matrix materials. Emphasis is given to the state-of-the-art cluster deposition system, designed and built by our research group, as well as to its unique abilities. Moreover, case studies on two cluster-assembled nanocomposite material systems (Fe/Ag_m and Fe/Cr_m) prepared with this method are presented. Finally, an outlook on research directions for cluster-assembled nanocomposites is discussed.

1. Introduction

Composites are engineered multiphase materials, which are produced by combining at least two components. The combination of the distinct characteristics of the constituents gives rise to superior functional material properties of the composites compared to its constituents. One of the earliest man-made composite materials that shaped ancient civilizations is the mud brick (straw-reinforced clay).[1] Mankind has extensively used natural materials to produce composites such as bows,[2] mortar, and concrete.[3] The modern era of composite materials began with the birth of the synthetic plastic industry in the 20th century. For example, the combination of glass fibers with polymers has resulted in extremely strong lightweight products. Since then, composites have advanced and entered our daily lives in many ways due to their superior properties, such as reduced weight, higher durability, added functionality, and freedom in design. Researchers are now pushing the limits of composite materials in the field of nanocomposites, in which per definition at least one of the constituents of the composite exhibits dimensions in the nanometer range.[4] Work on modern nanocomposites progresses fast and many of them find applications in numerous areas from energy[5] to medicine.[6]

Similar to conventional composites, nanocomposites are classified according to their matrix materials, which can be polymers, ceramics, and metals.[7] Their functionality depends on the intrinsic properties of individual constituents as well as the size and size distribution of the secondary nanophase embedded in the matrix and the homogeneity of phase distribution.[8–10] Therefore, it is of great importance to have precise control over the synthesis parameters during fabrication of nanocomposites. While the production method depends strongly on the class of the nanocomposite, the critical element in the method is always the control over the dispersion of the secondary nanophase in the matrix material. Many solid-, liquid-, and gas-phase synthesis methods and their combinations have been used for the production of nanocomposite materials.[7] Some of the production methods require even postprocessing steps such as consolidation and heat treatment to obtain the desired properties of the nanocomposites.[11] Especially, the conventional metallurgy methods to fabricate metal/metal nanocomposites require complex thermomechanical steps, i.e., quenching and annealing, combined with plastic deformation.[12] Even though these conventional production methods have resulted in metal/metal

Dr. C. Benel, Dr. T. Reisinger, Dr. R. Kruk, Prof. H. Hahn
Institute of Nanotechnology (INT)
Karlsruhe Institute of Technology (KIT)
Hermann-von-Helmholtz-Platz 1, 76344 Eggenstein-Leopoldshafen,
Germany
E-mail: cahit.benel@kit.edu; thomas.reisinger@kit.edu;
robert.kruk@kit.edu; horst.hahn@kit.edu
Prof. H. Hahn
KIT-TUD Joint Research Laboratory Nanomaterials
Technical University Darmstadt
Otto-Berndt Str. 2, 64287 Darmstadt, Germany

(nano)composites with improved material properties, they need high energy input and long processing times.[13] Furthermore, the size, the width of size distribution, the micro(nano) structure, and the chemical composition of the dispersed nanophase and the matrix are defined by the thermodynamical characteristics of the alloy system and formation kinetics. Therefore, the design of new nanocomposite systems is restricted when the conventional metallurgy methods are employed.

One way to overcome such limitations is to fabricate nanocomposites through nonequilibrium processing techniques.[14] Among many of such techniques, physical vapor deposition (PVD) methods have been used intensively to fabricate nanocomposites, since they offer higher control over process parameters and in turn the features of the nanocomposites. One of the most promising PVD methods is magnetron sputtering, in which many basic process parameters including substrate temperature, substrate ion current density, bias voltage, partial pressure of the reactive gas (in case of reactive magnetron sputtering), the number of magnetron targets, the compositions of targets, and magnetic field balancing of the targets affect the grain size of the nanophase in nanocomposite films.[15–17] The chemical composition of the nanocomposite films can be controlled via codeposition using multiple evaporation sources for the individual elements and alloys.[18] However, the formation of the multiple-phase nanocomposite microstructure is essentially dependent on the immiscibility of the materials being deposited.[19,20] In the case of miscibility, alloy formation during the deposition is inevitable. Furthermore, the control over the size and size distribution of the secondary nanophase is limited. In some cases, a postannealing step is required to obtain the desired nanocomposite nanostructure.[21]

The simultaneous deposition of preformed clusters with a molecular beam of another element/compound/alloy (matrix material) onto a substrate offers a way to overcome the aforementioned limitations.[12,22] Today's cluster ion beam technology offers a great degree of control over the fabrication of clusters with defined size, size distribution, and chemical composition. Moreover, the possibility to explore several deposition scenarios with variable cluster impact energies onto substrates can lead to the potential control of the morphology of the clusters. Therefore, the combination of cluster ion beam technology and various PVD techniques provides new methods to realize cluster-assembled nanocomposites with functional properties, which are conventionally impossible to fabricate.

2. Cluster Ion Beam Deposition of Nanocomposites

There is a rich literature concerning the formation of cluster beams in ultrahigh-vacuum systems, mass-selection techniques, and deposition of clusters onto surfaces. Technically, the choice of cluster production depends on the type of cluster material and desired cluster beam characteristics. The most common cluster formation methods are gas aggregation, magnetron sputtering, laser ablation, arc discharge, and electrospraying,[23] all of which rely on the condensation of the supersaturated vapor to form clusters.[24] Typically, the size

Cahit Benel received his Ph.D. in Material Science and Engineering from Technical University Darmstadt under the supervision of Prof. Horst Hahn. He currently works as a postdoctoral researcher at the Institute of Nanotechnology, Karlsruhe Institute of Technology. His research interests focus on the design, fabrication, and characterization of nanoparticle- and cluster-assembled nanomaterials to investigate structure–property relationships. He is also involved in the study of advanced energy conversion, energy storage, and catalysis.

Thomas Reisinger was awarded his Ph.D. in Nanophysics in the group of Prof. Bodil Holst at the University of Bergen, Norway, following an M.Sc. in Physics from the Technical University of Graz, Austria, and a B.Eng. in Computer Science from the University of Edinburgh, Scotland. He is currently pursuing his Habilitation as a postdoctoral researcher in the group of Prof. Horst Hahn at the Institute of Nanotechnology, Karlsruhe Institute of Technology. His research interests include nanofabrication and matter–wave interference experiments. His current research focus is on properties of nanoparticle- and cluster-assembled thin films, including new applications in superconducting circuits.

Horst Hahn has been the Executive Director of the Institute for Nanotechnology at Karlsruhe Institute of Technology (KIT) since 2004. He obtained his Ph.D. from the Technische Universität Berlin in 1982. After a postdoc at Universität des Saarlandes, he moved to the United States and held several positions at Argonne National Laboratory, University of Illinois at Urbana-Champaign, and Rutgers University. He has been a full professor at the Technische Universität Darmstadt since 1992. His research is focused on defects and diffusion in metals and ceramics, nanostructured and amorphous materials, tailored and tunable properties of nanostructures, and energy materials and printed electronics.
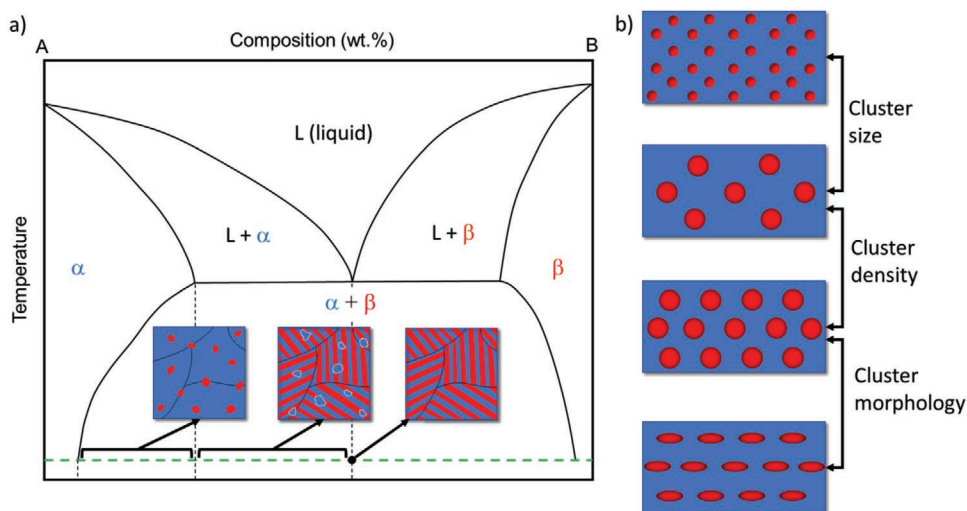
Figure 1. Comparison between the microstructures that can be obtained from conventional metallurgy methods and from codeposition of preformed clusters with a matrix material. a) Typical phase diagram for a binary eutectic system (A–B) showing different types of microstructures of composite materials obtained upon cooling of the molten alloy. b) Illustration of various cluster-assembled nanocomposites consisting of elements A and B in the phases of α and β, respectively, which can be realized using the CIBD method described in this work. The degree of control of cluster size, cluster density (fraction of clusters or overall composition), and cluster morphology in the cluster ion deposition approach is greatly improved compared to any other deposition method.

distribution of clusters obtained from different sources is wide. For most of the practical applications, a narrow distribution of cluster size is required. Therefore, the clusters are mass-selected by several methods, which widely vary depending on clusters' state of charge, mass range, and desired mass resolution. In terms of deposition of clusters onto surfaces, the precise control over the kinetic energy of clusters offers a potential way to control the shape and morphology of clusters.[25] Typically, three impact energy regimes are defined for clusters,, i.e., low energy (0.1 eV per atom), medium energy (1–10 eV per atom), and high energy (>10 eV per atom).[23] In the most trivial case, in which diffusion of the clusters on substrate surfaces and intermixing between cluster and substrate materials are prevented (typically by cooling down the substrate using liquid N_2), the low impact energy would result in minimally distorted clusters and substrate. On the other hand, at medium impact energies, the morphology modification for clusters and some defects on substrates are expected. At high energies, the clusters get fragmented and substantial damage of the substrate has been observed.[23] The technological advances in the field of cluster deposition technology and their combination with various thin-film deposition techniques offer new pathways to overcome the limitations in the nanocomposite material design, which are typically imposed by thermodynamics. **Figure 1** illustrates the limitations of conventional metallurgy methods (Figure 1a) in comparison to the freedom of design in the cluster deposition technology with regard to control over the microstructural features of the composite materials (Figure 1b).

We have used the cluster ion beam deposition (CIBD) system recently developed in our laboratory to realize a number of cluster/matrix nanocomposites.[12,26] A schematic of the CIBD system with all its functional units is presented in **Figure 2**. The clusters are produced in a magnetron sputtering/inert gas aggregation cluster source[27] (Figure 2a), in which the

size distribution of clusters is fine-tuned by the composition of sputtering gas (Ar/He), the aggregation length (distance between the sputter head and iris—at the latter the clusters
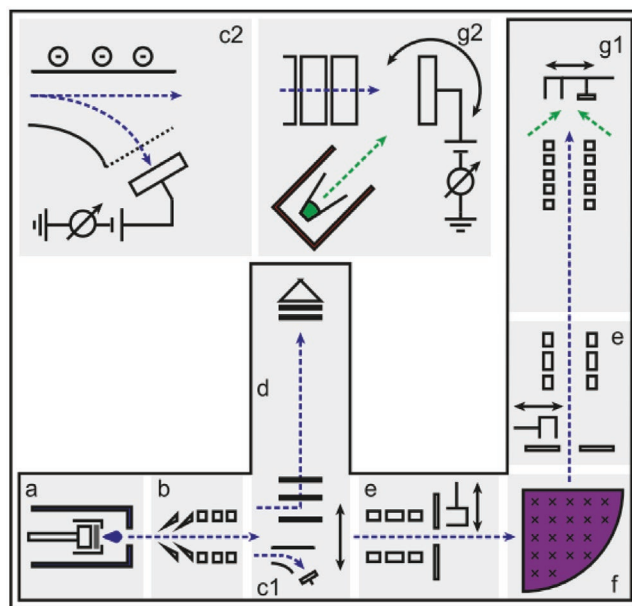
Figure 2. Schematic representation of the cluster ion beam deposition system with all its functional units. a) Cluster source. b) Differential pumping and acceleration lenses. c1) Sample holder for deposition of as-prepared clusters. d) Time-of-flight mass spectrometer. e) Quadruple triplet, selection slit, and Faraday cup detector. f) 90° sector magnet. g1) Deposition chamber with deceleration lenses, sample holder, Faraday cup, and (e-beam and thermal) evaporation sources (shown with green arrows). c2,g2) Detailed representations of the units of (c1) and (g1), respectively. Reproduced with permission.[26] Copyright 2015, AIP Publishing LLC.

1806634 (3 of 8)

exit the aggregation zone together with the inert gas into high vacuum), the aggregation pressure (the pressure within the aggregation zone), and the magnetron sputtering power. The ionized clusters are further accelerated by a set of electrostatic lenses (Figure 2b) to form a cluster ion beam to be deposited on substrates in a first deposition stage (Figure 2c). The mass distribution can be analyzed using a time-of-flight mass spectrometer (Figure 2d). Alternatively, the clusters can be mass-selected using a combination of two electrostatic quadrupole triplets (Figure 2e) and a 90° sector magnet (Figure 2f). Finally, the mass-selected clusters can be decelerated and deposited in a second deposition stage (Figure 2g).[26] The CIBD system allows the fabrication of a variety of cluster-assembled materials such as purely cluster-assembled materials (typically at the first deposition stage, without precise size selection), surface alloys, and cluster-decorated surfaces. However, those types of materials are out of scope for this manuscript. Therefore, such materials will not be discussed in the following sections. Typically, the cluster-assembled nanocomposites are fabricated in the second deposition stage (Figure 2g), in which a set of electrostatic lenses are used to focus the ion beam and to explore several deposition scenarios (by means of acceleration and deceleration) for the clusters. The CIBD system is capable of producing a wide range of clusters with sizes from a few to several thousand atoms per cluster, yielding several hundred nanograms of mass-selected clusters in a few hours. A wide range of materials and their combinations as matrix materials can be codeposited with mass-selected clusters using additional evaporation sources: a high-temperature effusion cell and a triple e-beam evaporator with three independent sources. The amount of deposited material is monitored by means of a quartz crystal monitor for the matrix material, whereas the cluster amount is monitored by counting the impinging charges using a picoamperemeter connected to the substrate.[26]

The unique capabilities of the CIBD system, therefore, give us the ability to design cluster-assembled nanocomposite materials with simultaneous control over several features. Potentially, the CIBD system can produce amorphous/crystalline metallic/semiconducting clusters embedded in metallic, semiconducting, ionic, or covalent matrices. In addition to such freedom of material choices, it offers close control over the cluster density in matrix, cluster size, and cluster deposition energy.

3. Size-Selected Clusters in Matrices

The properties of the clusters and the performance of the final nanocomposite product are highly dependent on the cluster size and its distribution. Therefore, the precise size selection of the clusters is the crucial step in the nanofabrication of the nanocomposites. In the most straightforward case, the clusters and the matrix materials are not interacting. In this case, the function of the matrix is to prevent the clusters from agglomerating and sintering with each other. Moreover, the protection of the clusters against oxidation is another functionality of the matrix material in this case. Second, in addition to the above-mentioned functions, the matrix can also add extra functionality to the resulting nanocomposite. To demonstrate the capabilities of the CIBD system, size-selected Fe clusters are embedded

in Ag and Cr matrices. In addition to the elemental analyses giving insight into homogeneity and precision of the cluster counting, the detailed magnetic characterizations of the samples are also carried out, since the magnetic properties of clusters are sensitive to their size, cluster density within the matrix, and cluster–matrix interactions.[28] The initial experiments deal with Fe clusters in Ag matrix for two main reasons. First of all, ferromagnetic (FM) Fe clusters would interact minimally with the diamagnetic Ag matrix in terms of magnetic interactions.[26] Second, Fe and Ag are immiscible. Therefore, minimal magnetic and chemical interactions are expected for this case study. On the other hand, a more complex nanocomposite, Fe clusters in Cr matrix, is also investigated, in which Fe clusters are coupled magnetically to the antiferromagnetic (AFM) Cr matrix via exchange interactions. The absolute amount of Fe deposited is the same for all the Fe/Ag_m and Fe/Cr_m samples. An equivalent Fe thickness of 6 nm is realized for the Fe clusters, whereas the Fe cluster concentration of different samples is adjusted by the amount of the deposited Ag and Cr matrix materials.[12] The thickness of the nanocomposite films thus ranges from 12 nm (50 vol% Fe samples) to 300 nm (2 vol% Fe samples).

3.1. Fe Clusters in Ag Matrix

To investigate the number of the deposited clusters, cluster homogeneity, and their magnetic properties, several Fe_x/Ag samples with 2, 10, 50 and 100 vol% Fe_{1000} (Fe cluster with 1000 atoms per cluster) were synthesized in the low impact energy regime.

The amounts of the deposited Fe clusters and the spatial distribution of the Fe clusters within the Ag matrices are investigated by means of energy-dispersive X-ray spectroscopy (EDX) measurements. **Table 1** shows that the actual Fe concentration of the Fe/Ag nanocomposites deviates from the nominal values (the targeted concentration values in the experiments) by only 10%. Further EDX analysis over the entire surface of the sample (**Figure 3**) indicates that the Fe clusters are deposited homogeneously within the intended part of the substrate. Both results demonstrate clearly the unique capabilities of the developed CIBD system in terms of control over the chemical composition and sample homogeneity.[26]

The superparamagnetism of the Fe/Ag nanocomposites is investigated using a superconducting quantum interference device (SQUID) magnetometer, since the magnetic features of the samples can give insights into the other relevant sample characteristics such as cluster size, magnetic cluster amount, and

Table 1. EDX measurements of the sample compositions for the various Fe_{1000}/Ag samples. Reproduced with permission.[26] Copyright 2015, AIP Publishing LLC.

Nominal volume percentage of Fe in Ag	Actual volume percentage of Fe in Ag (measured with EDX)
2	1.8 (2)
10	9 (1)
50	48 (5)
100	–
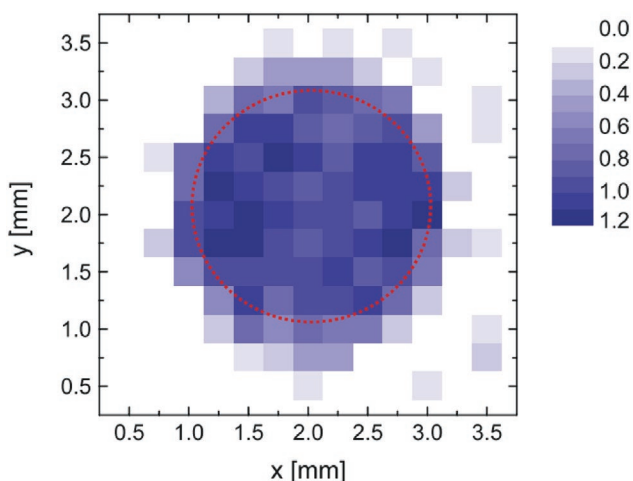
Figure 3. Elemental map of the Fe concentration in a typical Fe_x/Ag_m sample recorded using EDS. The nominal Fe concentration was normalized to 1. The red circle indicates where the Fe clusters are deposited through a mask with 2 mm diameter. Pixels close to the edge of the mask's opening may indicate false amounts of Fe, since they were just partially covered. Reproduced with permission.[26] Copyright 2015, AIP Publishing LLC.

cluster morphology (aggregation of clusters). The standard zero field cooled/field cooled (ZFC/FC) measurements (**Figure 4**a) show that the most diluted sample (2 vol%) shows a $1/T$ dependence for temperatures above the blocking temperature, T_B. This indicates that the Fe clusters are well separated within the Ag matrix and they interact minimally with each other. On the other hand, the 10 and 50 vol% Fe samples exhibit an increase in T_B, which suggests the presence of enhanced magnetic interaction among Fe clusters within the Ag matrix and even the formation of agglomerations. The sample consisting of only Fe clusters without any Ag matrix (100 vol% Fe) shows a minor variation of magnetization as the temperature changes, which suggests that this sample displays a magnetic behavior similar to that of a Fe thin film. To evaluate the amount of the magnetic Fe clusters within the Ag matrix, the magnetization loops of the samples are measured at 5 K after field cooling the sample with an applied magnetic field of $\mu_0 H = 4.5$ T (Figure 4b). An additional thin-film sample consisting of the same amount of Fe is also compared with cluster-assembled Fe/Ag nanocomposites. Although all the samples consist of same Fe amounts, the normalized saturation magnetization, M_s, values deviate from each other. For the sample having the lowest vol% of Fe clusters, the M_s is found to be ≈110 emu g_{Fe}^{-1}. The values of M_s increase as the cluster fraction within the matrix increases. The maximum M_s values of ≈190 emu g_{Fe}^{-1} are obtained for the fully cluster-based and thin-film Fe samples, which are comparable to the M_s of bulk Fe, 220 emu g_{Fe}^{-1}.

The discrepancy between the spectroscopic Fe amount obtained from EDX analyses and the magnetic Fe amount deducted from magnetic characterization can be explained in several ways such as oxidation of Fe clusters, formation of nonmagnetic phase (face-centered cubic Fe), and partial or complete mixing of Fe and Ag. Indeed, there is a sign of oxidation in all cluster-assembled nanocomposites. The magnetization loops measured at 5 K are horizontally shifted (not shown in
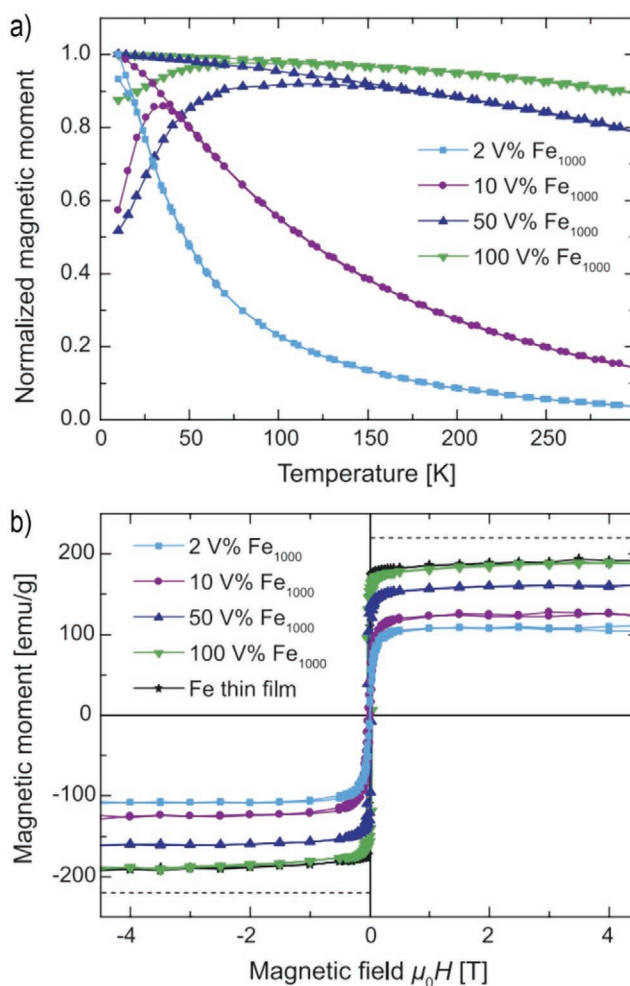
Figure 4. a) ZFC/FC curves of Fe_{1000} cluster/Ag matrix samples with 2, 10, 50, and 100 vol% Fe. The ZFC/FC curves are measured using a SQUID magnetometer with an applied magnetic field of $\mu_0 H = 20$ mT. b) Magnetization loops of Fe_{1000} cluster/Ag matrix samples with 2, 10, 50, and 100 vol% Fe and of Fe thin film with the same nominal Fe amount as that of the cluster-assembled nanocomposites. Black dotted lines indicate the magnetic moment of bulk Fe: 220 emu g_{Fe}^{-1}. The measurement is conducted at 5 K after field cooling the samples from 300 K in a magnetic field of 4.5 T. All data are corrected for linear (para- or diamagnetic) background. Reproduced with permission.[26] Copyright 2015, AIP Publishing LLC.

Figure 4b), which results from the exchange bias (EB) effect (the interfacial coupling of a ferromagnet with an antiferromagnet or ferrimagnet—see also next section). The formation of ferrimagnetic Fe_2O_3 and/or Fe_3O_4 must be taken into account for the reduced saturation magnetization values. However, the measured exchange bias is relatively low for any potential Fe/Fe_xO_y system, which might be existing in Fe/Ag nanocomposite samples. This suggests that only a small fraction of Fe clusters is oxidized. Second, the possibility of formation of any nonmagnetic Fe phase is also unlikely as transmission electron microscopy (TEM) experiments suggest. Finally, the formation of a solid solution between Fe and Ag might explain the relatively lower saturation magnetization for the nanocomposites having low Fe cluster fractions. Although Fe and Ag are immiscible, the higher surface areas of the small Fe clusters might

**ADVANCED
SCIENCE NEWS**

www.advancedsciencenews.com

**ADVANCED
MATERIALS**

www.advmat.de

facilitate local formation of solid solution between Fe and Ag. Further experiments such as atom probe tomography and detailed TEM analysis might explain the reason of magnetically missing Fe clusters.
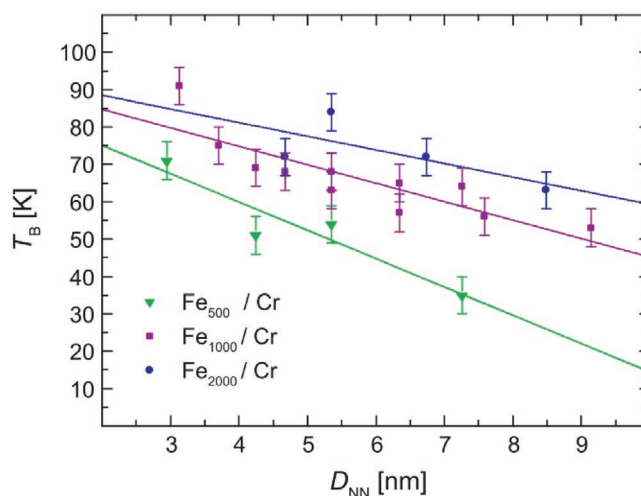
3.2. Fe Clusters in Cr Matrix

Following the promising results from the comparatively simple nanocomposite of Fe clusters in Ag matrix, we have used the CIBD apparatus to study a more complex material system.[12] It is composed of FM Fe clusters in an AFM Cr matrix. As in the case of Fe/Ag, the two elements are essentially immiscible at room temperature for most compositions according to their binary phase diagram. The resulting material system is, however, more complex in the sense that the magnetic interaction between clusters and matrix is no longer negligible. Its magnetic properties are thus expected to be strongly dependent on cluster size and cluster density in the matrix. Therefore, this cluster–matrix material system, although it has been studied in the literature before,[29] is a good choice for demonstrating that the cluster-size selective CIBD method can be used to finely tune material properties.

Choosing AFM Cr instead of diamagnetic Ag as the matrix material for the nanocomposite invariably affects its magnetic properties on a macroscopic scale. The main idea is that the coexistence of a FM and an AFM phase leads to spin exchange coupling at their interfaces. The result is that the magnetic moments of a soft FM phase become partially pinned, yielding an increased magnetic anisotropy. This unidirectional anisotropy manifests itself as an exchange bias,[30] namely, a horizontal shift of the magnetization loop by H_{eb}. The shift occurs when the system is field cooled down from a temperature above the Néel temperature (T_N) of the AFM phase and below the Curie temperature (T_C) of the FM phase ($T_C > T > T_N$) to a temperature below T_N. The effect is normally accompanied by an increase in coercivity (H_c) and blocking temperature (T_B).[31]

Meiklejohn and Bean were the first to observe and describe the EB effect in core–shell nanoparticles with diameters between 10 and 100 nm and composed of a FM cobalt core and an AFM cobalt oxide shell.[32] Since then numerous, including some more recent, studies have demonstrated the effect in core/shell clusters,[33,34] thin-film systems,[35,36] and cluster/matrix combinations.[29,37,38] The EB effect leads to an increase of thermal stability of the FM phase, resulting in an increase of the particle blocking temperature, and thus allows pushing the superparamagnetic limit to smaller particle size. This is, for example, of importance in ultrahigh-density magnetic recording.[30]

To determine the influence of cluster size and cluster density, a number of samples with Fe_x/Cr nanocomposite films have been prepared using the CIBD apparatus. The Fe cluster ions were codeposited at low energy (≈50 eV per cluster), corresponding to the soft-landing regime, together with Cr evaporated using an effusion cell. The samples were cooled close to liquid nitrogen temperature during deposition to avoid cluster agglomeration. The series includes samples of three different cluster sizes (500, 1000, and 2000 Fe atoms per cluster) within a wide cluster density range (2–50 vol% Fe). Great care was taken to avoid contamination and oxidation of the films by


Figure 5. Blocking temperature T_B vs approximated average cluster nearest-neighbor distances D_{NN} for thin films composed of Fe clusters in a Cr matrix. The shown data points represent samples with cluster sizes of 500, 1000, and 2000 atoms, corresponding to estimated cluster diameters of 2.3, 2.8, and 3.6 nm, respectively. The variation in D_{NN} corresponds to cluster volume fractions from 2 to 50 vol%. It can be seen that T_B increases with cluster size and decreases with D_{NN}. Reproduced with permission.[12] Copyright 2015, Beilstein-Institut.

maintaining a pressure of 10^{-9} mbar in the deposition chamber and sandwiching the nanocomposite layer by pure Cr layers and at the end covering the sample by an additional Au film.

The TEM study conducted on a representative sample (10 vol% Fe_{1000}/Cr) clearly showed that the Fe clusters were uniformly distributed in the Cr matrix and no significant agglomeration was observed. Furthermore, the sizes of the Fe clusters were estimated to be ≈3 nm, which matches the expected 2.8 nm. Additional diffraction data from TEM revealed that the Fe clusters as well as the Cr matrix both retain the body-centered cubic (bcc) structure as expected. Further details on this TEM study can be found elsewhere.[12]

After preparation, the samples were analyzed in a commercial SQUID magnetometer (Quantum Design). Standard ZFC/FC magnetization data and magnetic hysteresis loops were recorded, with the magnetic field applied parallel to the sample surface. The temperature range was between 10 and 350 K.

First the blocking temperature was determined from the ZFC/FC data for the various samples. The result is shown in **Figure 5**, where T_B is plotted against cluster nearest-neighbor distances (D_{NN}) that were inferred from the cluster volume fraction in the matrix. A bcc arrangement of the clusters was assumed to this end. An approximately linear effect of D_{NN} can be observed within the investigated region, where the slope is shallower for larger clusters. From a simple model of noninteracting clusters, a linear relation of the type $T_B \propto K_{eff}V$ is to be expected, where K_{eff} is an effective anisotropy constant and V the particle volume. The blocking temperatures in the experimental series also tend to increase with cluster size. Compared to bulk α-iron, the anisotropy constants estimated from the data are almost two orders of magnitude larger. Furthermore, the blocking temperatures are up to almost an order of magnitude larger when compared to samples of comparable cluster

**ADVANCED
SCIENCE NEWS**

www.advancedsciencenews.com

**ADVANCED
MATERIALS**

www.advmat.de
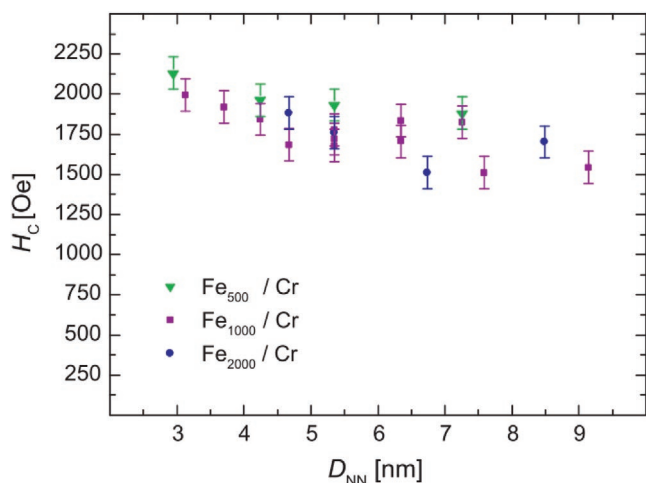
Figure 6. Coercivity H_c vs approximated average cluster nearest-neighbor distances D_{NN} for the same Fe_x/Cr samples as shown in Figure 5. The investigated samples do not reveal a dependence on cluster size; however, a weak trend toward smaller coercivity for increasing D_{NN} can be observed. Reproduced with permission.[12] Copyright 2015, Beilstein-Institut.

size and volume concentration in the Fe/Ag data series. These pieces of evidence allow the conclusion that FM/AFM exchange coupling is the likely source of the enhancement in the magnetic anisotropy of the Fe/Cr samples.

In **Figure 6**, the measured coercivities of the samples are displayed as a function of D_{NN}. It was derived from the hysteresis loops. They were recorded at 5 K after field cooling from 350 K in an external magnetic field of $\mu_0 H = 4.5$ T. The elevated starting temperature was chosen since it is above the Néel temperature of Cr (311 K).[39] Any possible effect of the cluster size cannot be inferred from the data, but a marginal rise of the coercivity for small D_{NN} can be noted. This shows that the H_c largely depends on the local anisotropy of the Fe clusters and interactions between individual clusters only slightly add to coercivity. However, a comparison to the Fe/Ag system again shows a distinct relative increase in coercivity by at least an order of magnitude. The hysteresis loops (not shown) also reveal a reduced saturation magnetization (e.g., ≈ 65 emu g_{Fe}^{-1} for the 10 vol% Fe_{1000} samples), which can be easily explained by a bilayer of frustrated (canted) spins at the interface between the FM/AFM phases. These prevent full saturation of the hysteresis loops, resulting in an additional linear term that is hard to extract from the data due to the also present diamagnetic background.

For the same hysteresis loops, the exchange bias H_{eb} was extracted. This is shown in **Figure 7** as a function of D_{NN}. The data do not show any dependence on D_{NN}, but a smaller cluster size can be seen to increase H_{eb}. To understand this behavior, a rudimentary model is devised. It is based on the idea that the spin exchange coupling occurs at the interface between the FM and the AFM phase only, whereas the torque induced on the magnetization of the FM clusters by the external magnetic field depends on the total magnetic moment per cluster and is thus related to cluster volume. The result is a behavior of $H_{eb} \propto 1/R$, where R is the cluster radius. This corresponds beautifully to the observed average

change in H_{eb} with cluster size, as is shown in Figure 7b. The observation allows the conclusion that the exchange bias effect is a rather local effect limited to the interfacial region. A similar dependence has been derived and tested for analogous thin-film systems of Fe and Cr.[40]

4. Conclusions and Outlook

The conventional metallurgy methods have natural limitations in controlling the microstructure and chemical composition of the nanocomposite at the same time, since they typically depend on the phase diagrams of the composite systems. Non-equilibrium synthesis methods offer several advantages to overcome such limitations but the simultaneous control of the size, size distribution, chemical composition, and morphology of the secondary nanophase typically lacks precision. In some cases, a postsynthesis step is required to achieve the desired characteristics of nanocomposites. In comparison, the cluster beam deposition technology in combination with several PVD techniques offers unprecedented control over the micro(nano)structural features of the cluster-assembled nanocomposites, which have a major influence on their functional material properties. In this progress report, therefore, the idea of cluster-assembled nanocomposites prepared by using a state-of-the-art CIBD system along with the brief description of the system, its capabilities, and two representative cluster-assembled nanocomposite material systems (Fe/Ag and Fe/Cr) is presented. The elemental and magnetic characterizations of Fe/Ag nanocomposite show that the system is capable of fabricating cluster-assembled nanocomposites with precisely size-selected clusters with predetermined cluster amounts, which are homogeneously distributed within the Ag matrix. Having met these requirements, which are crucial for the design and fabrication of cluster-assembled
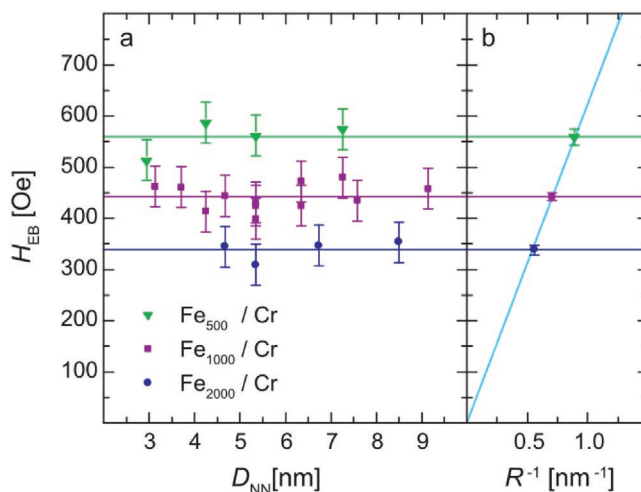
Figure 7. a) Exchange bias H_{eb} vs approximated average cluster nearest-neighbor distances D_{NN} for the same set of Fe_x/Cr samples. Cluster nearest-neighbor distances do not appear to influence exchange bias, but an increase in cluster size is associated with an increase in exchange bias. b) Average H_{eb} for the three cluster sizes vs inverse cluster radius R^{-1}: The linear fit clearly indicates a linear relation. Reproduced with permission.[12] Copyright 2015, Beilstein-Institut.

nanocomposites with advanced functional properties, a more complex nanocomposite material, Fe/Cr, is fabricated. The complexity of the system stems mainly from the magnetic interactions between ferromagnetic Fe clusters and antiferromagnetic Cr matrix, which manifests itself in the form of exchange bias effect. Several Fe/Cr nanocomposites are fabricated in a highly systematic and reproducible way, and their structural features such as cluster sizes and cluster volume fractions are correlated with their magnetic characteristics.

Both series of the experiments concerning the metal/metal nanocomposites show that the CIBD system offers a great potential to contribute to various fields in nanocomposite research. The control over the microscopic features results in the development of new nanocomposites with advanced functional properties, such as superconducting and spintronic materials. The former might be utilized to develop new superconducting nanocomposite circuits that can potentially find application in the field of quantum computing technology, while the latter have a wide range of applications such as magnetoresistive memory devices and magnetic field sensors. Although this state-of-the-art fabrication process is optimized for metal/metal nanocomposites, other classes of nanocomposites having ceramic and polymer matrices are possible to fabricate. Therefore, this method gives us the possibility to design a whole new set of nanocomposite materials beyond the limitations of today's synthesis methods.

Conflict of Interest

The authors declare no conflict of interest.

[1] S. Love, *Geoarchaeology* **2012**, *27*, 140.
[2] G. Gunduz, B. Yaman, S. Ozden, S. C. Donmez, *Sains Malays.* **2013**, *42*, 547.
[3] A. Moropoulou, A. Bakolas, S. Anagnostopoulou, *Cem. Concr. Compos.* **2005**, *27*, 295.
[4] S. Komarneni, *J. Mater. Chem.* **1992**, *2*, 1219.
[5] Y.-G. Guo, J.-S. Hu, L.-J. Wan, *Adv. Mater.* **2008**, *20*, 2878.
[6] E. Ruiz-Hitzky, M. Darder, P. Aranda, K. Ariga, *Adv. Mater.* **2010**, *22*, 323.
[7] P. Henrique, C. Camargo, K. G. Satyanarayana, F. Wypych, *Mater. Res.* **2009**, *12*, 1.
[8] F. Hussain, M. Hojjati, M. Okamoto, R. E. Gorga, *J. Compos. Mater.* **2006**, *40*, 1511.
[9] R. Casati, M. Vedani, *Metals* **2014**, *4*, 65.
[10] P. Palmero, *Nanomaterials* **2015**, *5*, 656.
[11] V. Viswanathan, T. Laha, K. Balani, A. Agarwal, S. Seal, *Mater. Sci. Eng. R: Rep.* **2006**, *54*, 121.
[12] A. Fischer, R. Kruk, D. Wang, H. Hahn, *Beilstein J. Nanotechnol.* **2015**, *6*, 1158.
[13] N. A. Luechinger, R. N. Grass, E. K. Athanassiou, W. J. Stark, *Chem. Mater.* **2010**, *22*, 155.
[14] C. Suryanarayana, *Prog. Mater. Sci.* **2001**, *46*, 1.
[15] S. Zhang, D. Sun, Y. Fu, H. Du, *Surf. Coat. Technol.* **2003**, *167*, 113.
[16] S. C. Velasco, A. Cavaleiro, S. Carvalho, *Prog. Mater. Sci.* **2016**, *84*, 158.
[17] S. Tamulevicius, S. Meskinis, T. Tamulevicius, H. Rubahn, *Rep. Prog. Phys.* **2018**, *81*, 024501.
[18] B. F. Faupel, V. Zaporojtchenko, T. Strunskus, *Adv. Eng. Mater.* **2010**, *12*, 1177.
[19] J. Musil, *Surf. Coat. Technol.* **2000**, *125*, 322.
[20] P. J. Kelly, H. Li, P. S. Benson, K. A. Whitehead, J. Verran, R. D. Arnell, I. Iordanova, *Surf. Coat. Technol.* **2010**, *205*, 1606.
[21] C. P. Luo, S. H. Liou, L. Gao, Y. Liu, D. J. Sellmyer, *Appl. Phys. Lett.* **2000**, *77*, 2225.
[22] A. Vahl, J. Strobel, W. Reichstein, *Nanotechnology* **2017**, *28*, 175703.
[23] C. Binns, *Surf. Sci. Rep.* **2001**, *44*, 1.
[24] V. N. Popok, I. Barke, E. E. B. Campbell, K. H. Meiwes-Broer, *Surf. Sci. Rep.* **2011**, *66*, 347.
[25] H. Haberland, M. Karrais, M. Mall, Y. Thurner, *J. Vac. Sci. Technol. A* **1992**, *10*, 3266.
[26] A. Fischer, R. Kruk, H. Hahn, *Rev. Sci. Instrum.* **2015**, *86*, 023304.
[27] H. Haberland, M. Mall, M. Moseler, Y. Qiang, T. Reiners, Y. Thurner, *J. Vac. Sci. Technol. A* **1994**, *12*, 2925.
[28] J. Bansmann, S. H. Baker, C. Binns, J. A. Blackman, J. P. Bucher, J. Dorantes-Dávila, V. Dupuis, L. Favre, D. Kechrakos, A. Kleibert, K. H. Meiwes-Broer, G. M. Pastor, A. Perez, O. Toulemonde, K. N. Trohidou, J. Tuaillon, Y. Xie, *Surf. Sci. Rep.* **2005**, *56*, 189.
[29] M. T. Qureshi, S. H. Baker, C. Binns, M. Roy, S. Laureti, D. Fiorani, D. Peddis, *J. Magn. Magn. Mater.* **2015**, *378*, 345.
[30] V. Skumryev, S. Stoyanov, Y. Zhang, G. Hadjipanayis, D. Givord, J. Nogués, *Nature* **2003**, *423*, 850.
[31] J. Nogués, I. K. Schuller, *J. Magn. Magn. Mater.* **1999**, *192*, 203.
[32] W. H. Meiklejohn, C. P. Bean, *Phys. Rev.* **1957**, *105*, 904.
[33] D. Peng, K. Sumiyama, T. Hihara, S. Yamamuro, T. Konno, *Phys. Rev. B* **2000**, *61*, 3103.
[34] C. Binns, M. T. Qureshi, D. Peddis, S. H. Baker, P. B. Howes, A. Boatwright, S. A. Cavill, S. S. Dhesi, L. Lari, R. Kröger, S. Langridge, *Nano Lett.* **2013**, *13*, 3334.
[35] E. J. Escorcia-Aparicio, H. J. Choi, W. L. Ling, R. K. Kawakami, Z. Q. Qiu, *Phys. Rev. Lett.* **1998**, *81*, 2144.
[36] R. Ciprian, M. Carbucicchio, G. Palombarini, *IEEE Trans. Magn.* **2010**, *46*, 432.
[37] D. Tobia, E. Winkler, R. D. Zysler, M. Granada, H. E. Troiani, D. Fiorani, *J. Appl. Phys.* **2009**, *106*, 103920.
[38] B. Kuerbanjiang, U. Wiedwald, F. Haering, J. Biskupek, U. Kaiser, P. Ziemann, U. Herr, *Nanotechnology* **2013**, *24*, 455702.
[39] E. Fawcett, H. L. Alberts, V. Y. Galkin, D. R. Noakes, J. V. Yakhmi, *Rev. Mod. Phys.* **1994**, *66*, 25.
[40] E. Restrepo-Parra, J. Restrepo, J. F. Jurado, C. Vargas-Hernandez, J. C. Riano-Rojas, *IEEE Trans. Magn.* **2009**, *45*, 5180.